15418	SHOCKED/MELTED BRECCIA ("ANORTHOSITIC GABBRO")	ST. 7	1141.0 g

INTRODUCTION: 15418 is an aluminous breccia ("anorthositic gabbro"), texturally unique among Apollo 15 samples. Its brecciated interior was shocked and shock-heated, and its rind vesiculated and melted. It contains a few large white clasts and was shocked ~4.0 b.y. ago. It was originally studied in a consortium headed by Tatsumoto.

15418 was collected from the summit of the subdued rim crest of Spur Crater, near several other rocks bigger than 10 cm, and may represent material from as deep as 20 m in the crater. The sample is blocky, subrounded, gray, and tough, with prominent exterior vesicles (Figs. l, 2). It has zap pits on all sides and was moderately buried. Its lunar orientation is known.

Figure 1. Macroscopic view of 15418 showing exterior vesicles and zap pits. S-71-45284

Figure 2. Sawn surface of end piece ,27, showing plagioclase-rich clasts, fine-grain-size, overall homogeneity, small vesicles, and concentration of vesicles at rim (especially on right hand side). S-75-33763

PETROLOGY: 15418 is considered an important sample as a unique aluminous breccia ("gabbroic anorthosite", ~70% plag.) and as such was described and depicted by PET (1972). Photomicrographs are shown in Figure 3. The PET (1972) description is only of the exterior, melted portion of the rock. The only comprehensive studies have been by Heuer's group (Heuer et al. 1972, Christie et al. 1973, and an especially detailed description by Nord et al. 1977) who studied the interior as well as the exterior, using optical, microprobe, and SEM methods. The interior was also studied by Sewell et al. (1974) who provided microprobe analyses, and Gleadow et al. (1974) who provided a description. The interior has a fragmental nature with some large crystals of plagioclase (~5 mm) and less common olivines (2 mm) in a finer-grained, fragmental and recrystallized matrix (Fig. 3d,e), which consists of olivine, orthopyroxene, clinopyroxene, and plagioclase. All are shocked, with aggregate extinction, but each fragment consists of a polycrystalline aggregate. TEM studies show evidence for their crystallization from glass or from partial recovery from heavily deformed preexisting crystals. The plagioclase (clasts and matrix) have a limited compositional range (An_{96-97}), and so do mafic grains (Fig. 4) (Nord et al. 1977). Similar analyses were also presented by Ahrens et al. (1973) and Sewell et al. (1974) (note that the latter authors inverted the headings of the clinopyroxene and orthopyroxene analyses). Some of the plagioclases have a

spherulitic or fibrous (wheat-sheaf) texture, from the devitrification of an originally glassy feldspar. Intracrystalline pores (100-1000 Å) are also common, and might result from volatiles or from the density contrast between devitrified and undevitrified glass. The exterior (Nord et al. 1977, PET 1972) is different, and includes an outer zone of flow-banded glass -- several subzones occur (Fig. 3a,b,c). Nord et al. (1977) summarized the history of the sample as shown in Table 1: an initial slow-cooled equilibration followed by brecciation. A second impact produced shock deformation, melting of the surface, and injection of glass along cracks. Following this, heating devitrified the thetomorphic and melt glasses, and caused some recovery of the silicates. Subsequent small-scale impact produced minor cracking. A similar history is deduced by Richter et al. (1976) who studied microcracks in exterior samples, finding several episodes of cracking as shown by cross-cutting relationships. Some are open, others are sealed with glass with a composition similar to the bulk rock (they quoted the Bansal et al. 1972 analyses as for 15415,51 instead of 15418,51). Glass in fractures was injected but shows no flow-banding; at the edges the glassy plagioclase of the host has crystallized. Open cracks were subjected to differential strain analysis (DTA). The crack closure pressures are similar to other lunar samples, but the porosity is low, and the cracks were produced in mild shock events.

Hutcheon et al. (1972) also used HVEM to study what was mainly a single large clast of plagioclase. It was highly deformed with an heterogeneous distribution of deformation, and abundant recrystallization. They found gas bubbles but no pre-existing (i.e., formed prior to the rock) solar flare tracks. Huffman et al. (1974) and Schwerer et al. (1973) tabulated Mossbauer and magnetic studies of the sample. Magnetic studies showed 0.067% metallic iron. Mossbauer studies showed none, all iron being in silicates: 59.5% in pyroxene, 40.4% in olivine, none in oxides or sulfides.

Studies of glass of 15418 composition were made by Cukiermann and Uhlmann (1972), Uhlmann et al. (1974), and Yinnon (1980). They studied flow characteristics, measuring viscosity v. temperature, reliable data only being obtained above 1270°C (no crystals) and below 835°C. At intermediate temperatures crystallization took place during the time required to measure viscosity. Uhlmann et al. (1974) also shows the variation of crystal growth rate with temperature. Yinnon et al. (1980) conducted differential thermal analysis (DTA) experiments, and plotted the crystallization temperature against the heating rate.

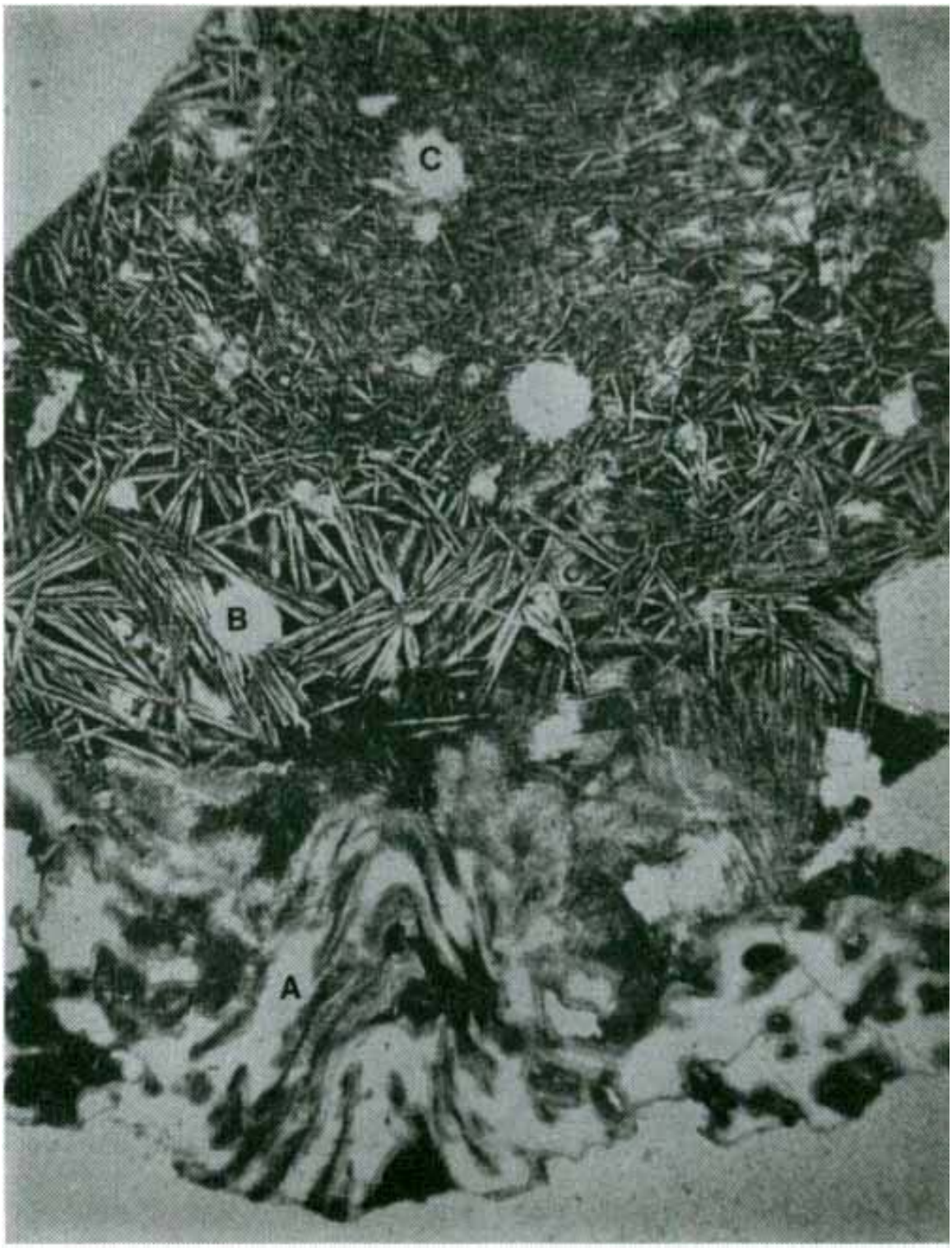

Fig. 3a

Figure 3. Photomicrographs, all to same scale except (c):
(a) 15418,8, exterior rind, with zones A, B, C described by Nord et al. 1977.
Transmitted light.

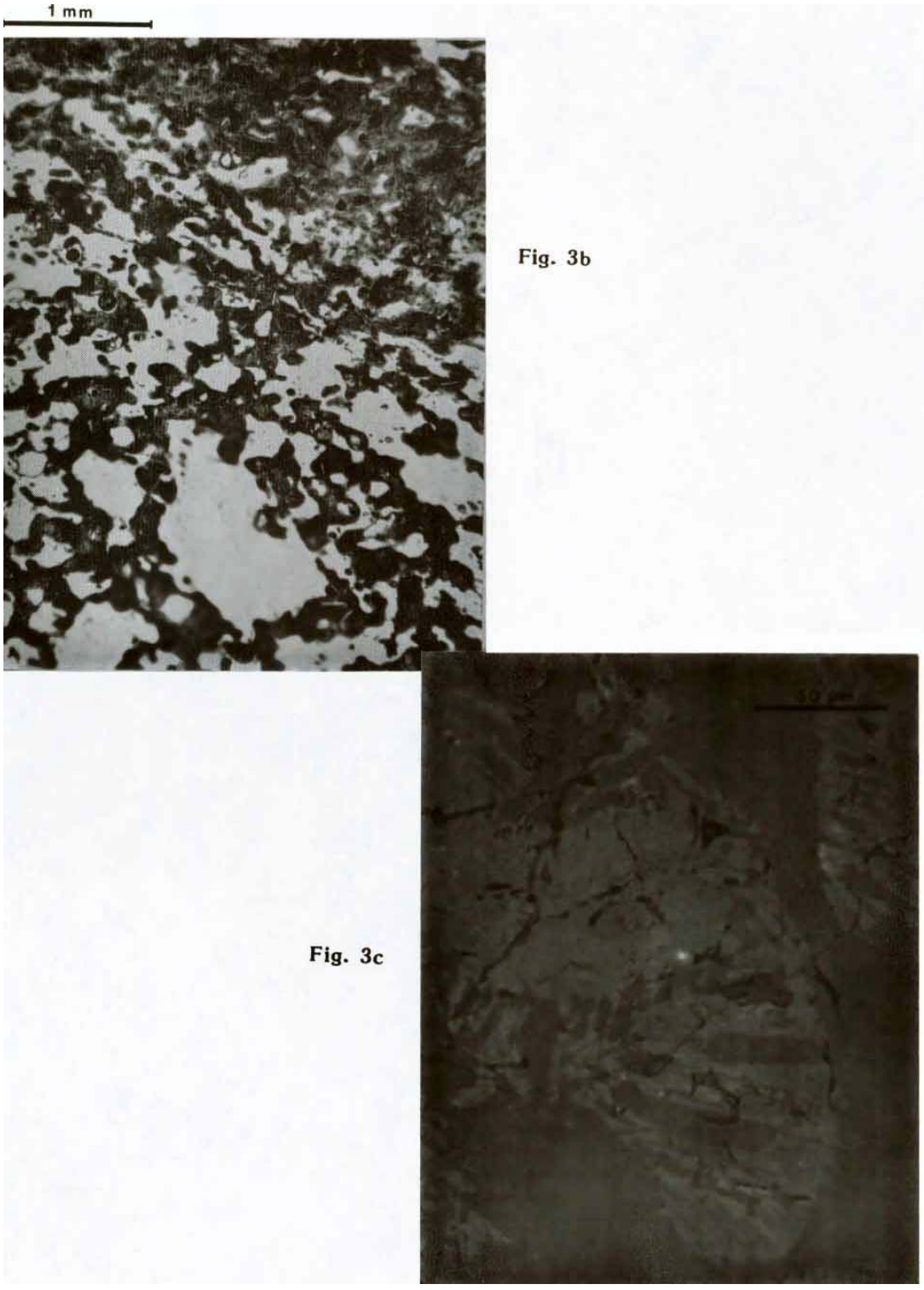

(b) 15418,17, more common exterior as manifested in thin sections and showing some similarities with the interior of the rock. White is plagioclase, dark is plag + px, all shocked and recrystallized. Transmitted light.
(c) 15418,17, detail of (b): lighter gray is mafic phases, darker gray is plagioclase. Reflected light.

Fig. 3d

Fig. 3e

(d) 15418,98, interior of 15418 showing fragmental and recrystallized texture; bottom left is a single larger plagioclase crystal. Transmitted light.
(e) 15418,98, same field as (d) but crossed polarizers, showing polycrystalline nature of grains.

TABLE 15418-1. Summary of mechanical and thermal history of 15418
(Nord et al., 1977)

Event	Mechanical effects	Thermal effects	Processes and resulting textures
I		Initial crystallization and slow cooling.	Coarse-grained texture. Chemical equilibration approached.
II a.	Fracturing and brecciation.	First impact event.	Brecciated structure.
b.		Shock heating	Recrystallization giving rise to present hornfelsic grain structure Chemical equilibrium established or undisturbed?
III a.	Shock deformation and ejection with partial melting of surface.	Second impact event.	Partial shock vitrification and high local deformation. Fractures filled with impact-produced melt from rock surface.
b.		Shock heating	Devitrification of thetomorphic and melt glasses. Recovery and partial recrystallization of deformation structure. Element distribution unchanged.
IV	Transport (farming) by small impacts.		Some cracking with little or no effects on fabric.

CHEMISTRY: Analyses are listed in Table 2, and rare earths plotted in Figure 5. Authors generally merely noted the aluminous and low-potassic nature of the sample. Some of the analyses are on sawdust from the slabbing. The major elements and rare earths are consistent among analyses, but some variation occurs in some trace elements e.g. between the two splits analyzed by Ganapathy et al. (1973). This difference is said to be a more probable result of different mineralogies than to have anything to do with vesicularity (Ganapathy et al. 1973).

Allen et al. (1973a,b) analyzed for ^{204}Pb and for Fe metal; the tentative values for ^{204}Pb in Allen et al. (1973b) were replaced. Hubbard et al. (1972) reported the same data as PET (1972) but differ in Na_2O (0.21% instead of 0.31%) and K_2O (0.05% instead of 0.03%). Their quote of 0.93% instead of 0.03% for P_2O_5 is undoubtedly a printing error.

RADIOGENIC ISOTOPES AND GEOCHRONOLOGY: Rb and Sr whole rock isotopic data is presented by Nyquist et al. (1972, 1973), Wiesmann and Hubbard (1975) and Tatsumoto et al. (1972) (Table 3). The data are reasonably consistent.

Stettler et al. (1973) did ^{40}Ar-^{39}Ar dating on the sample (Fig. 6) finding a high temperature plateau at 3.99 ± 0.07 b.y., and an intermediate temperature release age of 4.04 ± 0.06 b.y. The constancy of the Ca/K ratio indicates that the potassium is in plagioclase, not in an accessory phase.

Tatsumoto et al. (1972) reported Pb isotopic ratios and ^{238}U/^{204}Pb for one sample, and ^{232}Th/^{238}U for three samples including sawdust. The sample lies above concordia indicating lead enrichment relative to uranium in the sample analyzed. The data point for the sawdust is below concordia if the Pb value of the rock is used instead of the sawdust value (whose very high lead is sawcut contaminant).

TABLE 15418-2. Chemical analyses of bulk rock

			,51a		,30-08	,30-08	,5	,51	,30-07A	,49	,30,03	,30-07A	
Wt %	SiO2	44.97	44.2						45.53				
	TiO2	0.27	0.27	0.37					0.29		0.23	0.272	
	Al2O3	26.73	26.6	26.4					25.98				
	FeO	5.37	6.65	7.5					6.66				
	MgO	5.38	5.08	5.3					6.09				
	CaO	16.10	16.0	15.8					15.63				
	Na2O	0.31	0.27	0.282					0.31		0.32	0.30	
	K2O	0.03	0.013	0.011					0.03		0.0200	0.0236	0.0104
	P2O5	0.03							0.03				
(ppm)	Sc			12.7						7.0			
	V			42						18.0			
	Cr	750		1900						1150	614	628	
	Mn	620		660					770				
	Co			77						10.0			
	Ni									54.0			
	Rb		0.17					0.162			0.361	0.489	
	Sr	152	140					140.1			148		
	Y									5.4			
	Zr	67		180							30	35	
	Nb												
	Hf			0.8						0.16	0.8	0.6	
	Ba		19.2	70						20.0	24.4	28.9	
	Th									0.10	0.28	0.34	0.102
	U		0.045		0.016	0.036					0.078	0.094	0.043
	Pb									0.14			
	La		1.07	1.2						1.06	1.73	2.19	
	Ce		3.31							2.4		6.78	
	Pr									0.33			
	Nd		2.09							1.41	3.15	3.75	
	Sm		0.688	0.69						0.43	0.940	1.16	
	Eu		0.726	0.73						0.69	0.764	0.762	
	Gd		1.25							0.67	1.25		
	Tb			0.18						0.12			
	Dy		1.12	1.2						0.8	1.49	1.84	
	Ho									0.19			
	Er		0.85							0.59	1.04	1.24	
	Tm									0.1			
	Yb		0.74	0.81						0.6	0.907	1.12	
	Lu		0.120	0.12						0.09	0.143	0.176	
	Li				16						2.3	2.6	
	Be												
	B												
	C						11						
	N												
	S	300	400(b)						300				
	F												
	Cl				1.11								
	Br				0.52	0.39							
	Cu									2.0			
	Zn												
(ppb)	I				1.6								
	At												
	Ga									2200			
	Ge												
	As												
	Se												
	Mo												
	Tc												
	Ru					3.4							
	Rh												
	Pd												
	Ag												
	Cd												
	In												
	Sn												
	Sb												
	Te				6.3								
	Cs												
	Ta			90									
	W												
	Re												
	Os					9.3							
	Ir												
	Pt												
	Au												
	Hg												
	Tl												
	Bi												
		(1)	(2)	(3)	(4)	(4)	(5)	(6)	(7)	(8)	(9)	(9)	(10)

TABLE 15418-2 Continued

		,30-08	,30-05Dc	,30-06d	,50				
Wt %	SiO2								
	TiO2								
	Al2O3								
	FeO								
	MgO								
	CaO				15.54				
	Na2O								
	K2O				0.0066				0.0152
	P2O5								
(ppm)	Sc								
	V								
	Cr								
	Mn								
	Co								
	Ni								
	Rb		0.80	0.03					0.263
	Sr								134.6
	Y								
	Zr								
	Nb								
	Hf								
	Ba								
	Th					0.1272	0.1377	0.2077	
	U		0.185	0.024		0.0380	0.0394	0.0578	
	Pb					0.138	0.132	(1.927e)	
	La								
	Ce								
	Pr								
	Nd								
	Sm								
	Eu								
	Gd								
	Tb								
	Dy								
	Ho								
	Er								
	Tm								
	Yb								
	Lu								
	Li								
	Be								
	B								
	C								
	N								
	S								
	F								
	Cl								
	Br		0.055	0.075					
	Cu								
	Zn	2.74	0.82	0.49					
(ppb)	I								
	At								
	Ga								
	Ge		65	17					
	As								
	Se		56	25					
	Mo								
	Tc								
	Ru								
	Rh								
	Pd								
	Ag		0.59	1.4					
	Cd		1.7	2.4					
	In		0.29	0.18					
	Sn								
	Sb		0.50	0.16					
	Te		3.7	1.9					
	Cs		40	8					
	Ta								
	W								
	Re		0.38	0.13					
	Os								
	Ir		5.4	2.2					
	Pt								
	Au		1.00	0.26					
	Hg								
	Tl		0.21	0.095					
	Bi	<1.09	0.16	0.29					
		(11)	(12)	(12)	(13)	(14)	(14)	(14)	(14)

References for Table 15418-2

References and Methods:

(1) PET (1972); XRF, AAS
(2) Bansal et al. (1972); XRF, ID
(3) Laul et al. (1972a), Laul and Schmitt (1972); INAA
(4) Reed and Jovanovic (1972); RNAA
(5) Moore et al. (1972, 1973)
(6) Nyquist et al. (1972, 1973); ID/MS
(7) Hubbard et al. (1974); XRF
(8) S.R. Taylor et al. (1973); SSMS, ES
(9) Wiesmann and Hubbard (1975); ID/MS
(10) Keith et al. (1972); Gamma-ray spectroscopy
(11) Allen et al. (1973); leaching, RNAA
(12) Ganapathy et al. (1973); RNAA
(13) Stettler et al. (1973); MS
(14) Tatsumoto et al. (1972); ID/MS

Notes:

(a) sawdust
(b) from Hubbard et al. (1974)
(c) vesicular exterior
(d) dense interior
(e) indicates sawing contamination

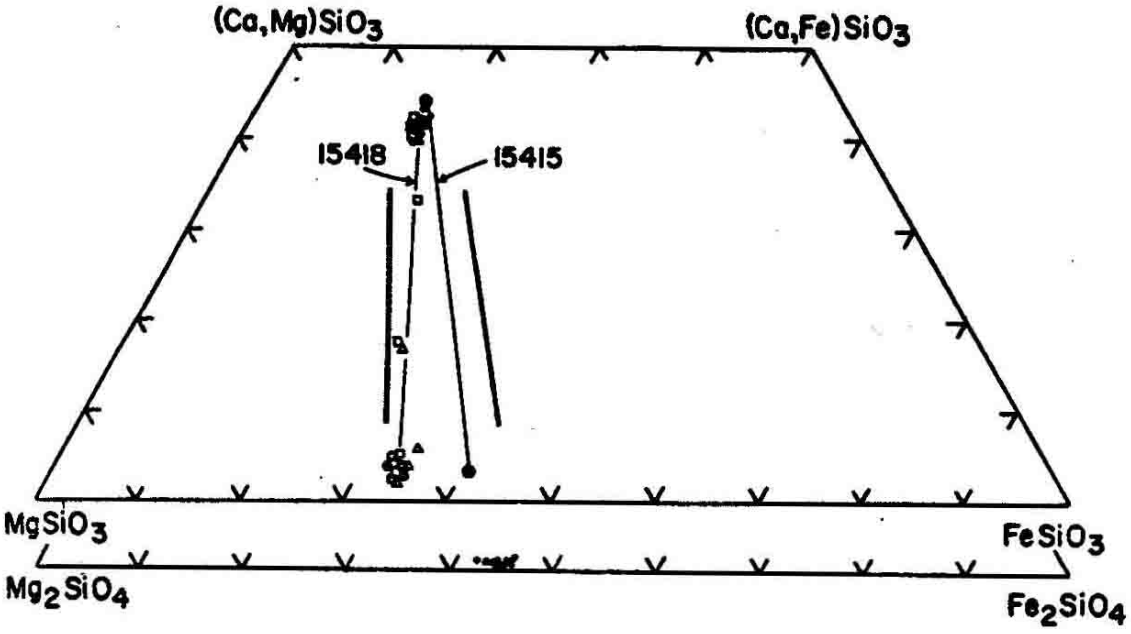

Figure 4. Pyroxenes and olivines in 15418,17 (Nord et al., 1977).

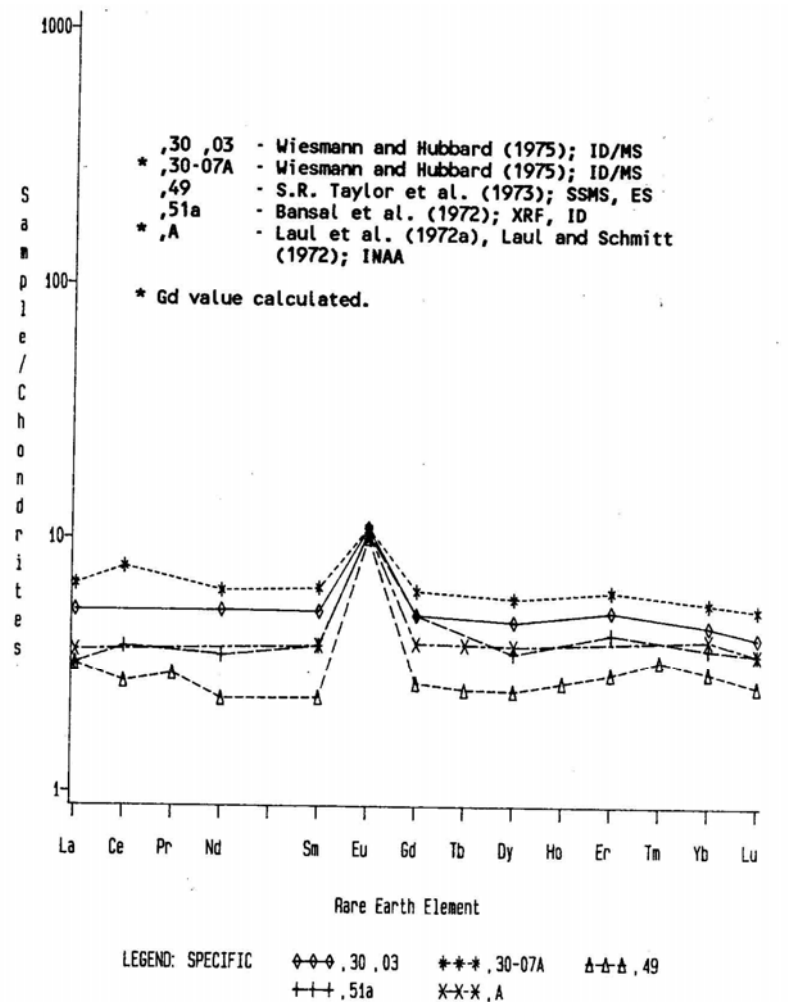

Figure 5. Rare earths in 15418.

EXPOSURE: Stettler et al. (1973) determined an exposure age of 250 m.y. using the ^{38}Ar method. Keith and Clark (1972) provided data on cosmogenic nuclides (with low ^{54}Mn, ^{56}Co, and ^{22}Na because of the calcic, mafic-poor nature of the sample). ^{26}Al is saturated, merely indicating exposure longer than 2 m.y. MacDougall et al. (1973) found no solar flare tracks in the sample.

PHYSICAL PROPERTIES: Nagata et al. (1972a,b, 1973, 1975) tabulated basic magnetic properties (hysteresis measurements) and NRM data. Kamacite is the major ferromagnetic constituent, with 4% Ni in the metal. The sample has an unusually small paramagnetic susceptibility. Demagnetization of ,46 revealed a hard component with an intensity of 1 x 10^{-6} emu/gm, with a direction reasonably constant for fields greater than 100 Oe.rms. Thermal demagnetization indicated an NRM attributable to a TRM acquired

by cooling from 300°C at most. The observed NRM of ,41 could be obtained with an impact pressure of 50 kb in a magnetic field of ~8000 gammas.

Todd et al. (1973) and Wang et al. (1973) tabulated seismic (Vp and Vs) measurement as a function of pressure (Table 4), finding the values similar to those for lunar igneous (mare) rocks. Ahrens et al. (1973) made Hugoniot measurements (Figs. 7,8), tabulating the data (Table 5) resulting from shock experiments. O'Keefe and Ahrens (1975) discuss the equation of state, and 15418 became the standard for lunar crustal impact modeling because of these data and its composition.

Schwerer et al. (1973, 1974) measured the electrical conductivity of 15418 in reducing and oxidizing atmospheres as a function of temperature (Figs. 9, 10) as well as produced Mossbauer spectra. Baldridge et al. (1972) measured the thermal expansion coefficients from -100°C to +200°C.

TABLE 15418-3. Whole rock Rb-Sr isotopic data
(not adjusted for interlaboratory bias)

Reference	Split	$^{87}Sr/^{86}Sr$	$^{87}Rb/^{86}Sr$
Nyquist et al. (1972, 1973)	,51 sawdust	0.69934 ± 5	0.0034 ± 3
Wiesmann and Hubbard (1975)	,30,03	0.69948 ± 12	
Tatsumoto et al. (1972)	,28,30, and/or ,51	0.69954 0.69965	

TABLE 15418-4. Seismic velocities (km/sec) as a function of pressure
(Todd et al., 1972) for 15418,43)

bars	1	100	250	500	750	1000	1500	2000	3000	4000	5000
P	4.85	5.00	5.20	5.50	5.77	6.02	6.33	6.50	6.64	6.69	6.75
S	2.82	2.88	2.97	3.08	3.19	3.28	3.42	3.50	3.58	3.63	3.69

TABLE 15418-5. Hugoniot data for lunar sample 15418 (Ahrens et al., 1972a).

Shot No.	Initial Density (g/cm³)	Flyer Plate Velocity (km/sec)	Elastic Shock Velocity (km/sec)	Free-Surface Velocity (km/sec)	Hugoniot Elastic Limit (kb)	Final Shock Pressure (kb)	Final Shock Density (g/cm³)
270	2.821	1.618[a] ±0.005	5.88 ±0.09	0.84	70±4	204±4	3.82±0.07
276	2.834	1.318[a] ±0.001	6.02 ±0.12	*	*	155±4	3.69±0.08
268	2.813	2.166[a] ±0.005	6.30 ±0.01	0.60	65±10	282±6	4.25±0.04
269	2.822	1.992[a] ±0.005	6.10 ±0.05	*	*	261±5	4.07±0.04
279	2.846	1.139[b] ±0.005	5.94 ±0.10	0.49	42±5	88±3	3.22±0.06
280	2.823	0.850[b] ±0.0015	6.04 ±0.05	0.56	48±5	65±2	3.08±0.05
281	2.812	0.803[b] ±0.002	6.18 ±0.02	0.61	53±2	63±1	3.03±0.01
277	2.821	1.020[a] ±0.005	5.99 ±0.04	0.84	71±10	129±7	3.37±0.06
287	2.823	1.17[a] ±0.006	6.24 ±0.11	0.65	57±6	148±8	3.48±0.08
288	2.806	1.108[a] ±0.005	6.14 ±0.02	0.80	69±11	145±7	3.38±0.04

[a]Polycrystalline W, 19.3 g/cm³.
[b]Aluminum alloy, 2024.
*Not measured.

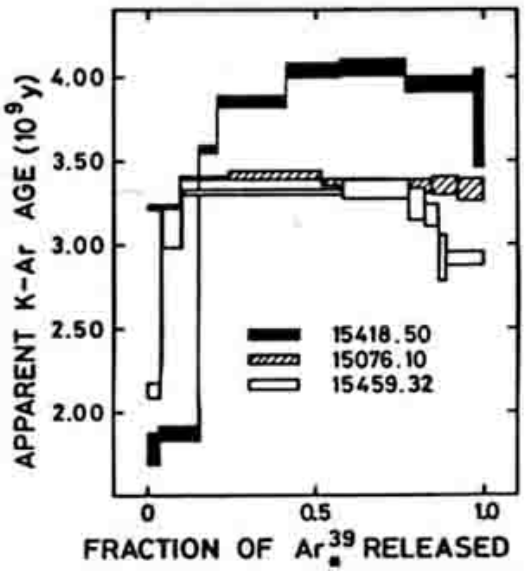

Figure 6. Ar release for 15418 and other samples

(Stettler et al., 1973).

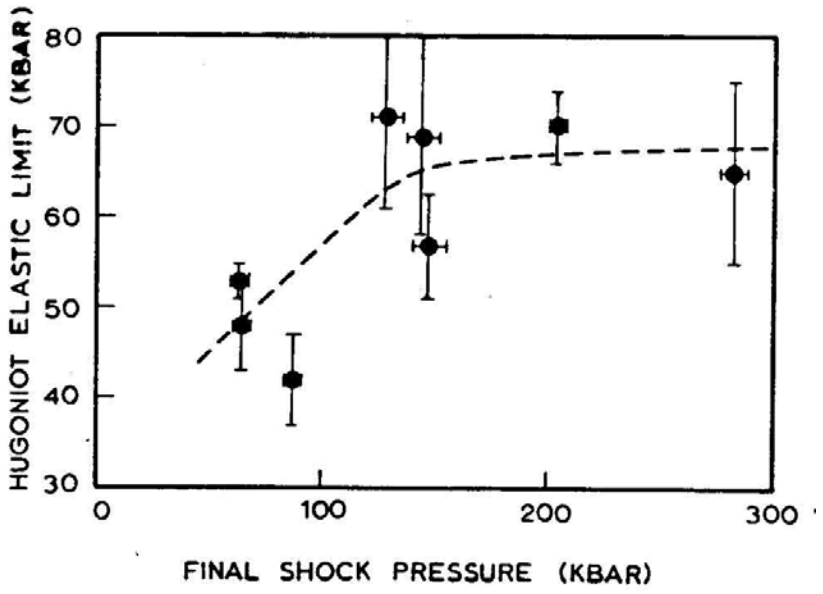

Figure 7. Hugoniot elastic limits as a function of shock pressure (Ahrens et al., 1973).

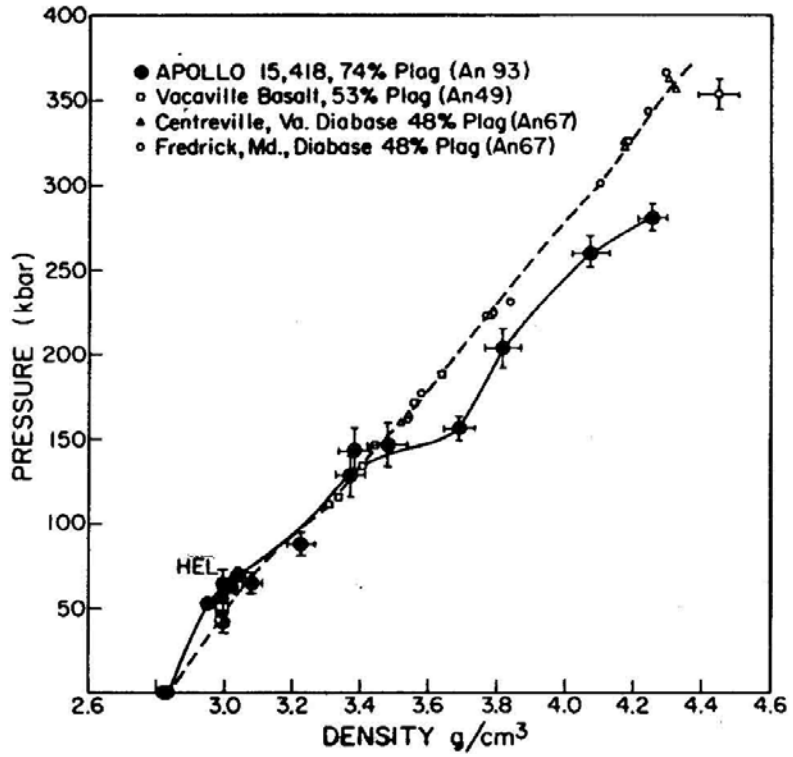

Figure 8. Hugoniot data for 15418 and several terrestrial analogs

(Ahrens et al., 1973).

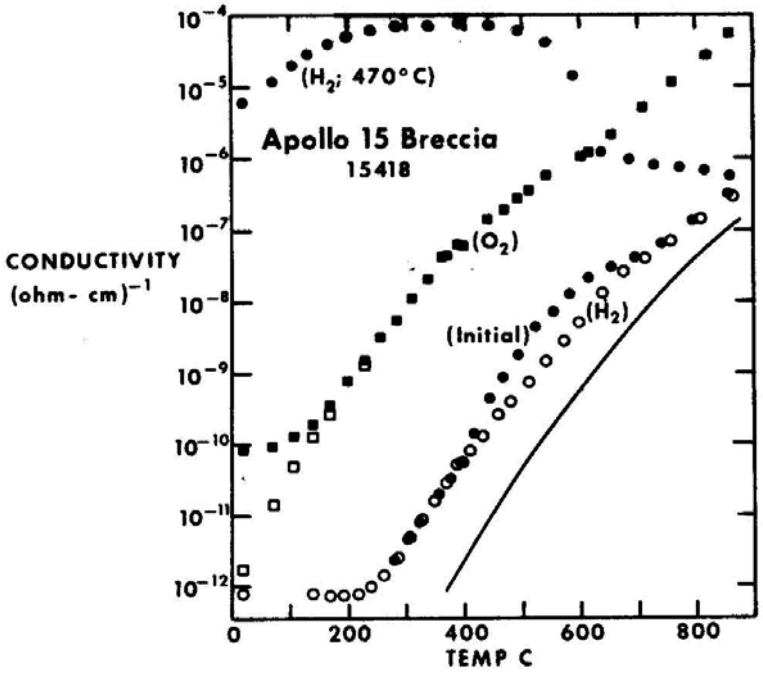

Electrical conductivity (dc) of lunar breccia (Apollo 15418) measured during initial heating, in reducing (H_2) and oxidizing (O_2) atmospheres, and in a reducing atmosphere after oxidation followed by low-temperature reduction (H_2; 470°C). Solid curve represents equivalent d-c leakage conductivity.

Figure 9. Electrical conductivity measurements (Schwerer et al., 1973).

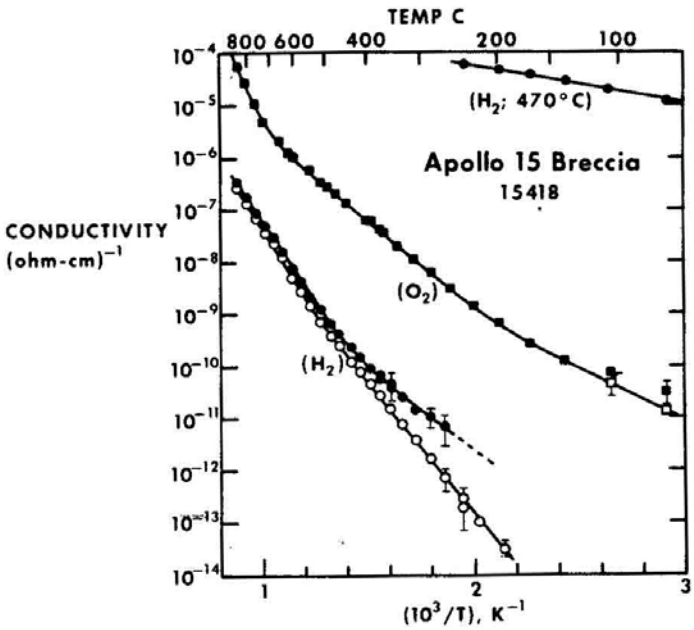

Electrical conductivity (dc, full symbols; ac, open symbols) of lunar breccia (Apollo 15418) in various atmospheres (*see* Fig. 4). Solid lines are results of least-squares fit to Equation 1 (*see* text).

Figure 10. Electrical conductivity measurements (Schwerer et al., 1973).
PROCESSING AND SUBDIVISIONS: Two chips, 1 and ,2 were originally taken from the exterior for allocation, including potted butt ,6 for thin sections ,8 and ,10 to ,26 (Fig. 11). Subsequently the rock was sawn, providing two end pieces which remain more or less intact: ,27 (321.3 g) now in remote storage, and ,0 (526.3 g) (Fig. 12). The slab piece ,28 was substantially subsawn, and ,28 and ,30 substantially split and allocated under the Tatsumoto Consortium and later studies. ,37 became a second potted butt, for thin sections ,152 to ,155. Thin section ,98 was made from ,47, an interior part of the slab taken from ,36.

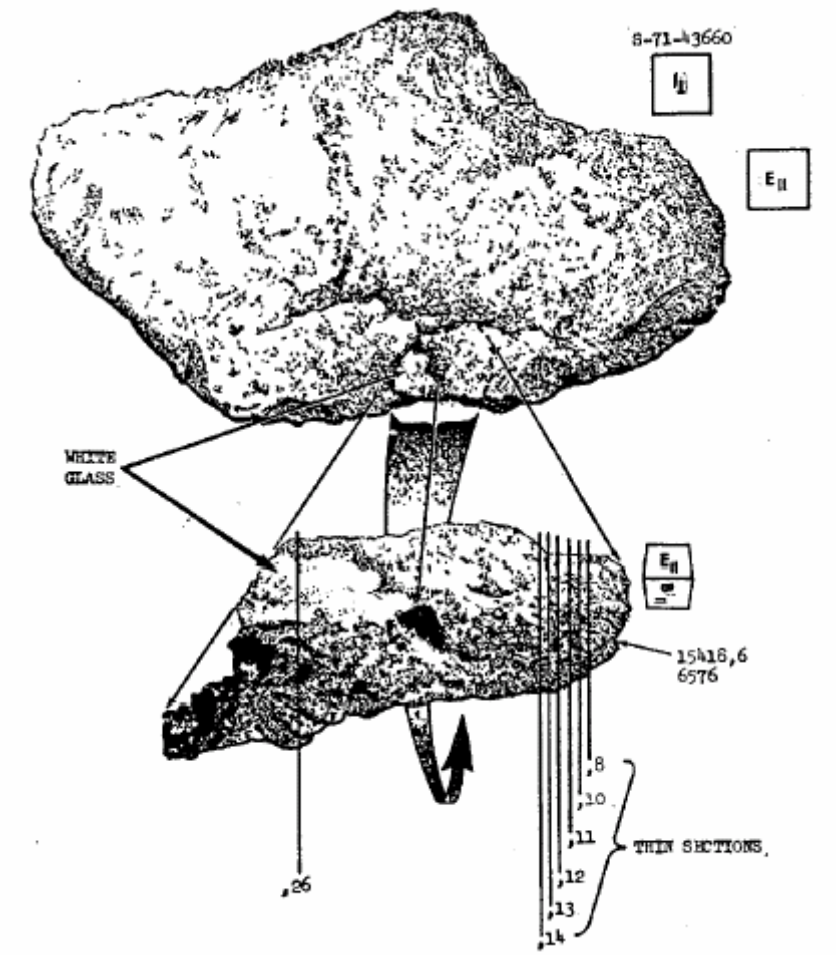

Figure 11. Potted butt ,6 and its thin sections.

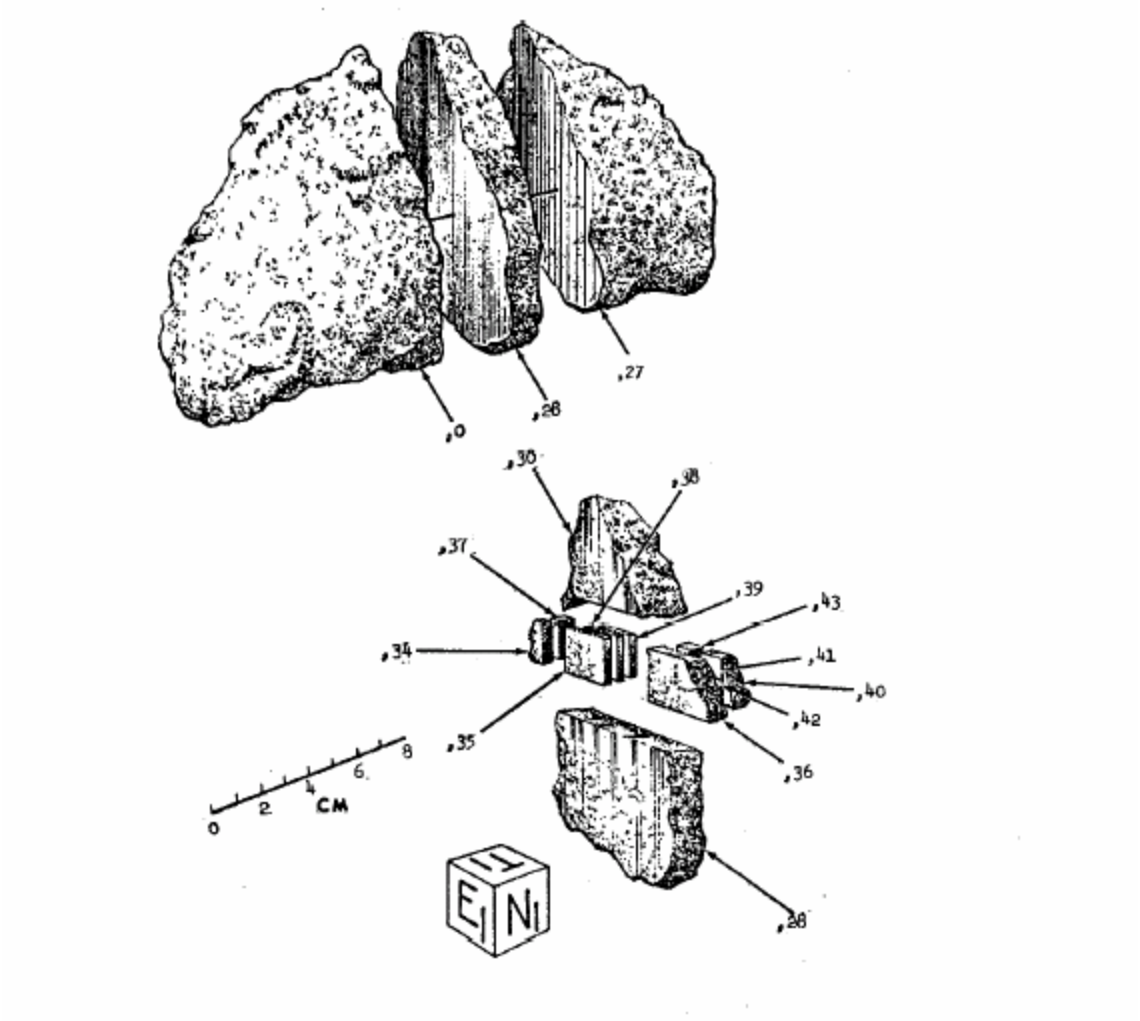

Figure 12. Main sawing subdivision of 15418.